Acta Crystallographica Section D
**Biological Crystallography**
ISSN 0907-4449

# Triple-axis X-ray diffraction analyses of lysozyme crystals

**H. M. Volz[a] and R. J. Matyi[b]***

[a]Materials Science Program, University of Wisconsin, Madison, WI 53706, USA, and [b]Department of Materials Science and Engineering, University of Wisconsin, Madison, WI 53706, USA

Correspondence e-mail: matyi@engr.wisc.edu

Received 10 January 2000
Accepted 11 April 2000

High-resolution triple-axis X-ray diffraction techniques have been used to monitor the defect structure in hen egg-white lysozyme crystals. Analyses from the (440), (1$\bar{2}$0) and (160) reflections showed significant differences in the intensity distribution around the respective reciprocal-lattice points. This work suggests that X-ray diffraction analytical methods developed primarily for relatively perfect inorganic crystals can be successfully applied to structurally defective macromolecular crystals. The analysis of defects at high angular resolution is complicated, however, by the observation that protein crystals lie at the convergence of the kinematic (ideally imperfect) and dynamic (ideally perfect) treatments of diffraction.

## 1. Introduction

The limiting factor in protein crystallography research is often obtaining high-quality X-ray diffraction data with good spatial resolution from a crystallized protein. In turn, the collection of diffraction data is frequently hindered by the inability to grow protein crystals with low defect concentrations. Defects and non-uniformities in proteins include dislocations, molecular heterogeneity, twinning, displacements arising from static or dynamic disorder, voids or bubbles, inclusions, slightly misoriented domains (mosaicity), impurities and strain (McPherson, 1999; Branden & Tooze, 1999). Some of these defects are exacerbated by X-ray damage incurred during characterization; the cryocooling employed to reduce the harmful effects of this radiation is known to broaden diffraction peaks.

Since the net diffracted intensity represents a summation over all atoms in the crystal, each atom displaced from its ideal equilibrium position owing to a defect in the structure serves to both reduce the intensity of a reflection and increase the diffuse scatter in the experiment. Typically, high-quality protein data have a spatial resolution of 2 Å or better. This resolution greatly impacts on the appearance of the electron-density map, which in turn affects whether individual atoms, molecules or no structure at all can be resolved. Elucidation of the factors that lead to the generation defects in protein crystals could lead to elimination of those defects, thereby improving both the spatial resolution of the structural determination and the subsequent analyses of protein functionality (McPherson, 1999; Branden & Tooze, 1999; Drenth, 1999).

It is instructive to contrast the state of the art in protein crystal growth with that of inorganic crystals such as semiconductor materials, where much progress has been made in recent years towards understanding the generation of defects during single-crystal growth. The quality of modern semi-

conductors (where the term 'high-quality crystal' implies an absence of structural defects) is considerably higher than that of protein crystals, partially as a consequence of the ability of researchers to correlate semiconductor growth conditions with the resulting defect structure. Semiconductors now routinely have defect densities that approach the thermodynamic limit. Through techniques such as high-resolution X-ray diffraction (HRXRD), information about crystalline quality can be readily obtained and rapidly fed back to the crystal-growth process (Loxley, 1994; Bowen & Tanner, 1998).

## 2. High-resolution diffraction methods for defect analysis

Whereas structural determination is generally the only use of X-rays to a protein crystallographer, researchers in the inorganic community have developed several characterization techniques to observe the behavior of defects in semiconductor structures. Two HRXRD methods that are commonly used involve double-axis rocking curves and triple-axis reciprocal-space maps. In the former method, monochromated X-rays impinge on a single-crystal sample positioned at the Bragg angle for a specific crystallographic reflection. The sample is then rotated by small amounts about an axis lying within those crystallographic planes and perpendicular to the plane of the diffractometer (also referred to as the $\omega$ axis or perpendicular to the reflection's reciprocal-lattice vector). Typical step sizes are sub-arcsecond to several arcseconds, with rotation ranges of the order of a fraction of a degree. The shape and breadth of the diffraction profile for a Bragg peak recorded with a stationary wide-open detector gives general information about crystalline quality and sample composition. Researchers often report the full peak width of the rocking curve at half the maximum intensity (FWHM) as a measure of crystalline perfection (Loxley, 1994; Bowen & Tanner, 1998).

Triple-axis X-ray diffraction can be envisioned as simply taking a series of these rocking curves, but instead of using a wide-open scintillation counter for a detector, the angular position of the diffracted beam is precisely defined through additional diffraction from an analyzer crystal with a very low defect density, typically high-quality silicon or germanium. Thus, the X-ray beam diffracts from at least three total crystals: the incident-beam conditioner (often a multiple-reflection crystal or collection of multiple-reflection crystals), the sample and a post-specimen analyzer crystal (Fig. 1). The

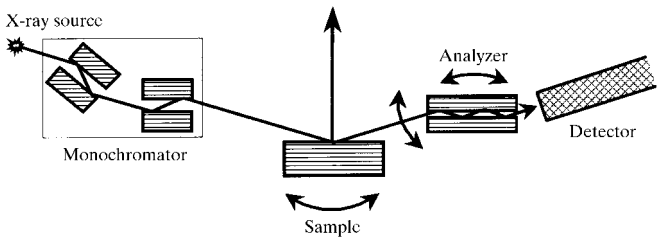


**Figure 1**
Schematic illustration of the triple-axis X-ray diffraction geometry.

superior angular resolution of this technique is critical for the observation of defect structure in crystalline materials. Usually this angular resolution is of the order of a few arcseconds, which is much finer than that which could be obtained with a simple collimator or narrow slit.

The effects of mosaic structure or other defects can be observed in conventional protein crystallographic analyses, but the detection limit for such distortions is limited by the angular resolution of the detector. The following rough calculation demonstrates this point. A high-quality area detector used for protein crystallography typically has a minimum pixel dimension of approximately 150 μm on a side, with a maximum sample-to-crystal distance of about 30 cm. In this favorable case each pixel would subtend an angle of 0.029° or about 100 arcsec. This is at least an order of magnitude inferior to the resolution that can be attained in a 'high-resolution' reciprocal-space map when a high-quality analyzer crystal is used.

An alternative approach to crystal defect characterization is to replace the electronic detector with high-resolution photographic film. When illuminated by X-rays, each diffracted beam can produce a so-called topographic image that contains information regarding the types, spatial distribution and densities of structural defects. X-ray topographic studies of protein crystals have been reported by Fourme *et al.* (1995), Izumi *et al.* (1996) and Stojanoff and coworkers (Stojanoff & Siddons, 1996; Stojanoff *et al.*, 1997). These studies have employed synchrotron radiation to produce perfect crystal monochromated topographs (Fourme *et al.*, 1995; Stojanoff & Siddons, 1996; Stojanoff *et al.*, 1997) and white-beam topographs (Izumi *et al.*, 1996; Stojanoff & Siddons, 1996; Stojanoff *et al.*, 1997). In all cases defects in lysozyme crystals were observed, but unambiguous defect assignments were difficult. This is often true of topographic images of structurally defective crystals, since their high defect densities mean that the images of individual defects may overlap, making interpretation difficult. The work by Stojanoff and coworkers (Stojanoff & Siddons, 1996; Stojanoff *et al.*, 1997) did demonstrate, however, that a decrease in the defect density as observed through topographic imaging correlated with an increase in structural resolution in subsequent crystallographic analyses. Recently, Dobrianov *et al.* (1999) have used X-ray topography to examine the effects of solution variations during growth, the influence of impurities and the use of post-growth treatments on protein crystals, while Otalora *et al.* (1999) have explored the mechanism of contrast variations in protein crystal topographic images.

Unlike topographic (imaging) techniques, non-imaging diffractometer methods can be applied to crystals with an arbitrarily high concentration of structural imperfections, making them a potentially very useful tool for studying protein crystals. In order to demonstrate this, we must discuss the effect of structural defects on a high-resolution diffraction experiment. Defects introduced into a crystal will alter the intensity distribution about a reciprocal-space point in two ways. First, compositional variations and/or strain in the lattice will locally change the lattice parameters of the sample. This

will be manifested in the redistribution of intensity away from the exact Bragg condition in the $\theta/2\theta$ direction (parallel to the direction of the reciprocal-lattice vector in a symmetric geometry, as shown in Fig. 2). Secondly, mosaic spread in the sample will create extra intensity away from the Bragg angle when rotating the sample axis $\omega$ (perpendicular to the reciprocal-lattice vector). The off-peak scattering that is associated with both factors can be measured in triple-axis diffraction and is usually graphed as a plot of equal-intensity contours (often called a reciprocal-space map), with one axis representing a rotation in $\omega$ and the other representing movement in $\theta/2\theta$.

Despite their benefits to the inorganic crystal growth community, there have been relatively few HRXRD analyses of protein crystals. One of the earliest systematic analyses of X-ray rocking curves from protein crystals was performed by Shaikevitch & Kam (1981). Using slit-collimated radiation from a sealed X-ray tube, they reported a mosaic spread of about 60 arcsec for a lysozyme crystal at $2\theta \simeq 15^\circ$. Recently, the advent of synchrotron sources with intense radiation and low divergence has led to a number of other X-ray rocking-curve analyses (Helliwell, 1988; Colapietro *et al.*, 1992; Snell *et al.*, 1995). Rocking-curve FWHM as narrow as 8.3 arcsec (0.0023°) from the (776) reflection has been reported for lysozyme crystals grown in microgravity (Snell *et al.*, 1995). This value is far superior to the approximately 47 arcsec FWHM observed in a similar crystal grown on earth.

The goal of the present work is to explore the use of high-resolution X-ray diffraction techniques (particularly high-resolution triple-axis methods) to the analysis of protein crystals. Recently, we have presented a preliminary HRXRD study of lysozyme crystals (Volz & Matyi, 1999). In the work described below, we have extended these analyses to explore the effects of different (*hkl*) reflections on the appearance of high-resolution reciprocal-space maps from protein crystals. It should be noted that our goal is to perform X-ray analyses that are characterized by high *angular* resolution, rather than the conventional protein crystallography goal of achieving a high *spatial* (*e.g.* '1.8 Å') resolution. Ultimately, this work should lead to insights into the strain and mosaic spread present in protein crystals *via* the tool of reciprocal-space mapping.

The protein chosen for our studies was hen egg-white lysozyme (HEWL), a well characterized protein frequently used in crystal-growth studies, partly as a consequence of its relative ease of crystallization. If successful, this work is expected to lead to a better understanding of the conditions that limit structural quality in protein crystal growth. Characterization of grown-in defects could lead to methods of reducing their densities, thereby increasing crystalline quality and improving the structural determinations that are central to the study of protein function.

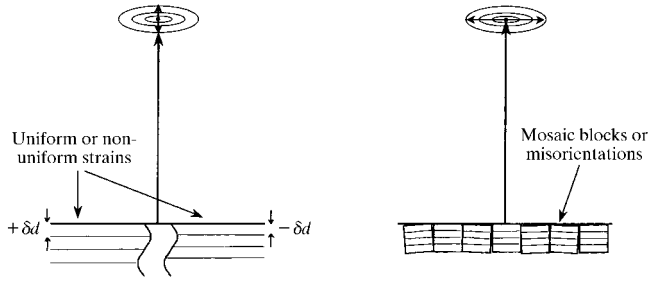


**Figure 2**
Schematic illustration of the effects of defects on the appearance of high-resolution reciprocal-space maps.

## 3. Experimental

### 3.1. Protein crystal samples

Samples of crystallized HEWL were obtained from Professor H. Holden and Dr. J. Thoden of the Institute for Enzyme Research at the University of Wisconsin–Madison. Crystals were grown at 298 K by microdialysis, a liquid–liquid diffusion technique. The lysozyme starting material was obtained from Sigma Chemicals and was used at a concentration of 40 mg ml$^{-1}$ in water. Dialysis was performed at pH 4.7 using 20 m*M* sodium acetate and 850 m*M* sodium chloride. Crystals of appreciable size typically grew within 2 d.

The HEWL crystals were tetragonal (space group $P4_32_12$, unit-cell parameters $a = 79.3$, $c = 38.1$ Å) with {101}-type facets visible. Each optically transparent crystal was mounted with a small amount of mother liquor in a 1 mm capillary, the ends of which were then sealed with wax before mounting with modeling clay on an eucentric goniometer.

### 3.2. High-resolution X-ray diffractometery

The characteristics of the instrumentation used to record transmission X-ray rocking curves and reciprocal-space maps has been described in depth elsewhere (Volz & Matyi, 1999). Briefly, a Huber 511/424 four-circle diffractometer, modified to permit a minimum step size of 0.00125° (4.5 arcsec), was used for all high-resolution analyses. Cu $K\alpha$ X-rays were generated by a Rigaku RU-200 rotating-anode generator configured with a point focus from a 0.5 × 10 mm focal spot. As shown in Fig. 3, the incident X-rays were conditioned by a

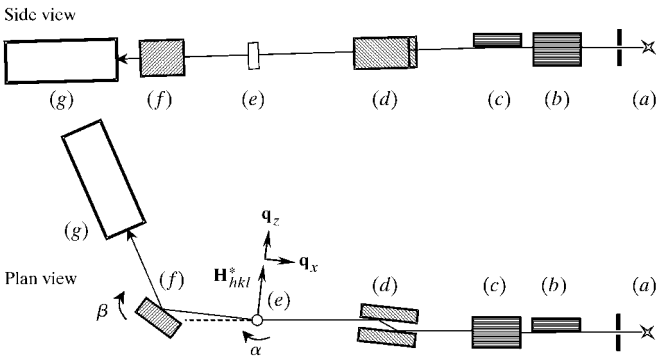


**Figure 3**
Illustration of the X-ray optical system configured for the analysis of defects in protein crystals: (*a*) X-ray source, (*b*) horizontal mirror, (*c*) vertical mirror, (*d*) channel-cut collimator, (*e*) sample, (*f*) analyzer, (*g*) detector. Also shown in the plan view are the angular deviations of the sample ($\alpha$) and analyzer ($\beta$) crystals and the sense of the deviation vectors $q_x$ and $q_z$ with respect to the reciprocal-lattice vector $\mathbf{H}^*_{hkl}$.

crossed pair of parabolic graded X-ray mirrors (Osmic, Inc., Troy, Michigan, USA). The crossed mirrors, which were situated in a novel X-ray optical system (Matyi *et al.*, 2000), produced a quasi-parallel X-ray beam (nominally 3 arcmin horizontal and vertical divergence) with an approximate beam dimension of 1 × 1 mm. The use of this crossed-mirror beam conditioner resulted in a significant increase in the incident beam X-ray flux as well as a two-dimensional collimation of the incident beam. Both effects were advantageous for the analysis of small weakly diffracting HEWL crystals in a conventional laboratory setting (Volz & Matyi, 1999).

Following conditioning by the crossed parabolic mirrors, the incident X-ray beam was further refined by diffraction from a grooved silicon crystal supplied by Bede Scientific. The two asymmetric (220) reflections served to condition the horizontal divergence of the X-ray beam from 3 arcmin to several arcseconds; the use of an asymmetric groove significantly increased the transmitted X-ray flux (Loxley *et al.*, 1995). The conditioned incident beam was then diffracted in transmission geometry from a HEWL crystal and the diffracted beam was analyzed by a single (004) reflection from a high-quality Ge[001] single crystal. Reciprocal-space maps of specific reflections were obtained by performing $\theta/2\theta$ scans with an increment in the sample angular position $\omega$ between scans.

Prior to the triple-axis diffraction experiments performed in this current study, the HEWL sample's orientation matrix was determined on a Syntex $P2_1$ diffractometer upgraded with Bruker–Siemens *P*3 software. Once the orientation matrix of a HEWL sample had been solved by this system, the specimen was then transferred to the four-circle Huber diffractometer. Since both of the diffractometers had been set up according to the same standard configuration, reflections generally could be found on the Huber diffractometer according to the angular positions supplied by the Syntex, with only minimal changes in sample rotation. We believe that the ability to reproducibly find reflections of a particular (*hkl*) was very important for consistency in our work.

## 4. Results

Fig. 4 shows two high-resolution triple-axis reciprocal-space maps that were recorded in our laboratory from an HEWL crystal in a prior preliminary analysis (Volz & Matyi, 1999). The reciprocal-space maps are plotted with contours of the logarithm of intensity, with each contour level representing $10^{0.25}$ counts $s^{-1}$ (*i.e.* four contours per decade of intensity). The angular (diffractometer) coordinates have been converted to orthogonal deviations ($q_x$, $q_z$) from the exact Bragg condition in reciprocal space using the relations

$$q_x = 2(\alpha - \beta)(\sin\theta/\lambda),$$
$$q_z = \beta(\cos\theta/\lambda), \quad (1)$$

where $\alpha$ and $\beta$ are the respective deviations of the sample and analyzer crystals from the exact Bragg condition, $\lambda$ is the wavelength of the X-rays used (Cu $K\alpha_1$, 1.54056 Å) and $\theta$ is the Bragg angle of the reflection. $q_z$ and $q_x$ correspond to directions that are parallel and perpendicular, respectively, to the reciprocal-lattice vector for a particular Bragg reflection. Note that the $q_x$ scale in all reciprocal-space maps has been expanded to assist the visualization of the intensity distribution around each reciprocal-lattice point.

The results of our prior analyses may be summarized as follows (Volz & Matyi, 1999). The reciprocal-space maps exhibit an irregular intensity distribution that is reminiscent of highly defective semiconductor crystals. Specifically, in Fig. 4(*a*) ($\theta_B = 3.16^\circ$) one can observe (i) a faint distribution of

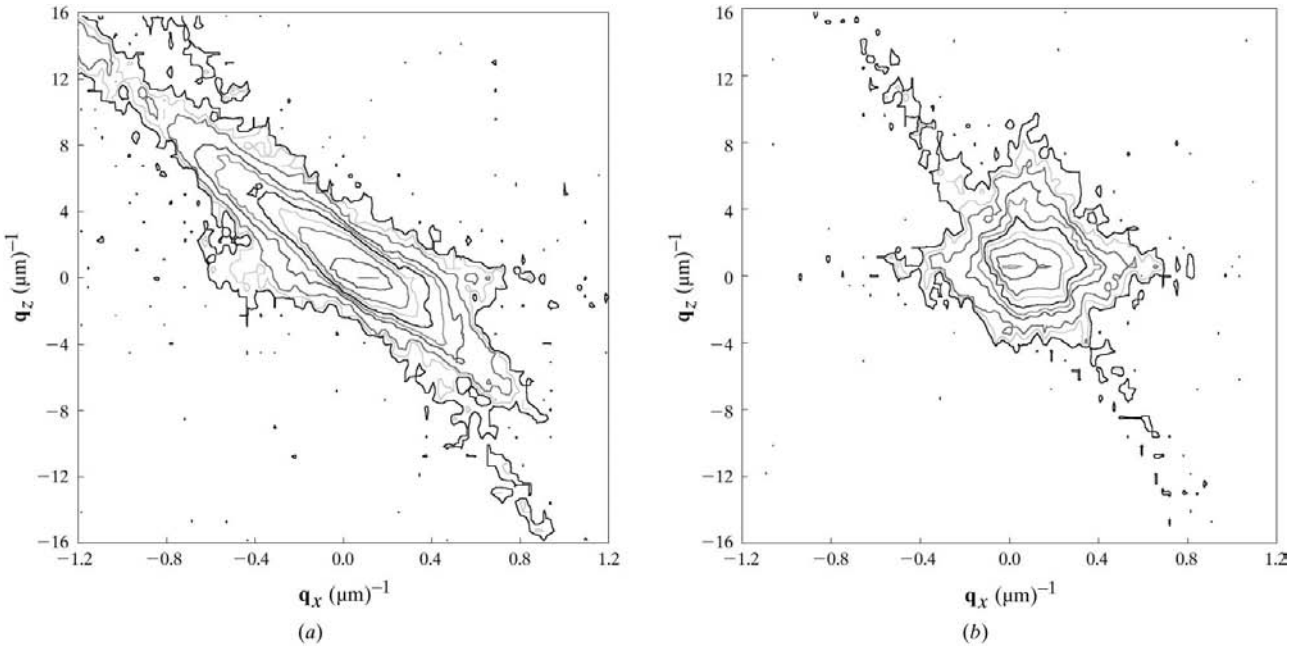


**Figure 4**
High-resolution triple-axis reciprocal-space maps recorded from two reflections with $\theta_B \simeq 3.16^\circ$ (Volz & Matyi, 1999).

intensity in the transverse direction (*i.e.* horizontally in the figure), (ii) an inclined relatively intense distribution extending from the upper left and through the reciprocal-lattice point towards the lower right and (iii) a weaker intensity distribution also extending from upper left to lower right in the figure but at a steeper angle. We believe that the third intensity of these cited above is the signature of parasitic scattering from our X-ray optical system, since it is evident in all reciprocal-space maps recorded from other reflections as well as other crystals. The other, more intense inclined feature is a 'surface streak', which is (as discussed below) the signature in a high-resolution diffraction experiment of the termination of the crystal lattice by the crystal surface.

Now let us consider the horizontal spread in intensity, which is believed to be a consequence of to the mosaic distribution in the HEWL crystal. Interpreted in this way, the mosaic spread of the crystal would thus be approximately 150–180 arcsec. It is important to note that this value corresponds to the *maximum* extent of the transverse off-peak scatter that was recorded from this crystal; in the parlance of a double-axis rocking curve, it would represent the full width at approximately 0.2% of the maximum intensity. Owing to the logarithmic intensity scale of the reciprocal-space maps, the full-width at half-maximum would correspond to a level that is between the second and third contour levels down from the maximum intensity and thus represents a value for the mosaic spread comparable with others in the literature.

It is doubtful that a measure such as this could be reliably made from a double-axis experiment, since there are numerous structural features that could alter the intensity distribution so far into the 'tails' of a rocking curve. However, the use of high-quality monochromator and analyzer crystals in high-resolution triple-axis diffraction reduces the spread in the direction and magnitude of the incident ($\mathbf{S}_0/\lambda$) and diffracted ($\mathbf{S}/\lambda$) wavevectors. This reduces the volume of reciprocal space that is sampled at any one time and leads to the separation of different types of off-peak scattering. As a result, weak intensity features (such as the angular extremes of scattering arising from mosaic spread discussed above) can be reliably and quantitatively described.

Fig. 4(*b*) shows a second reciprocal-space map recorded from the same crystal following a simple $\varphi$ rotation in the four-circle diffractometer. While the measured Bragg angle of this second reflection was also 3.16°, the difference between the two reciprocal-space maps is striking, with the only similarities being the inclined parasitic intensity from the crossed-mirror beam conditioner and the horizontal mosaic spread. We note that in Fig. 4(*b*) there is significant intensity distributed longitudinally (in the direction of the reciprocal-lattice vector, or vertically in the figure) indicating that there is a compressive strain in the crystal.

In this prior work the HEWL crystal was not pre-oriented and as a result the (*hkl*)s of the two reflections were not known. Hence, we have repeated our analyses utilizing known X-ray reflections on a second pre-oriented crystal. Figs. 5, 6 and 7 show the double-axis rocking curves and the triple-axis reciprocal-space maps that were recorded from three different reflections recorded from this second HEWL crystal. The reflections from this HEWL crystal were chosen based on their strong intensities during orientation on the Syntex diffractometer; the most intense were the (440), (160) and (1$\bar{2}$0) reflections. These specific (*hkl*)s were easily and reproducibly found on the Huber diffractometer from the orientation matrix calculated by the Syntex. The FWHM of the rocking curves from these reflections were narrower (45, 48 and 50 arcsec, respectively), suggesting a relatively high-quality crystallized enzyme (Shaikevitch & Kam, 1981; Helliwell, 1988; Colapietro *et al.*, 1992; Fourme *et al.*, 1995).

We note in passing that by pre-orienting the crystals in the current study, we ensured that the reciprocal-lattice vectors for the reflections in question were properly situated in the

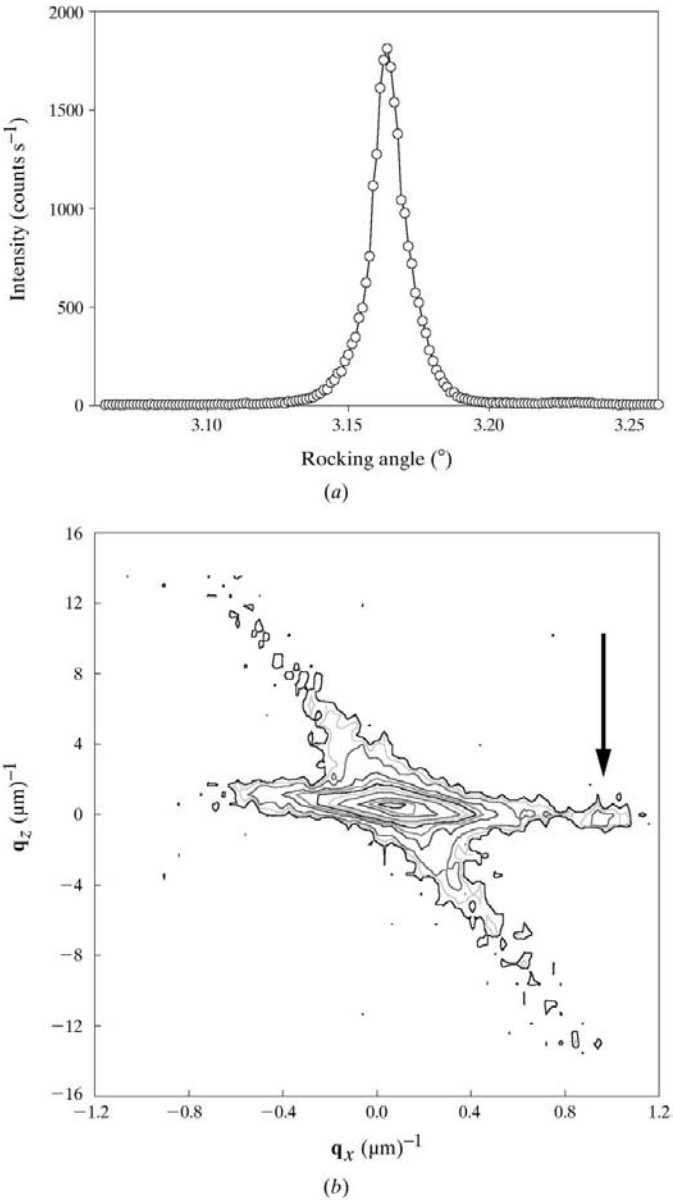


**Figure 5**
X-ray diffraction data from the HEWL (440) reflection. (*a*) Double-axis rocking curve (FWHM = 45 arcsec); (*b*) triple-axis reciprocal-space map (the arrow indicates the feature discussed in the text).

plane defined by the reciprocal-lattice vectors of the monochromator and analyzer crystals (*i.e.* in the plane of the diffractometer). A well known prerequisite for obtaining narrow double-axis rocking curves is that all diffracting planes must be parallel. Otherwise, there will be significant broadening of the measured reflection profile and the shape of the profile may be distorted (Bowen & Tanner, 1998). The preorientation procedure used in the present work thus ensures that an assessment of mosaic spread based on the rocking curve FWHM will indeed be representative of the crystal.

An examination of the reciprocal-space map from the (440) reflection (Fig. 5) shows that two definite intensity streaks can be clearly seen. The horizontal streak, as discussed previously, represents mosaic spread in the crystal. This result agrees well with observations in the protein crystal growth community that mosaicity is often present in these samples and serves to broaden diffraction peaks. Interestingly, there is an extra off-peak intensity feature (indicated by an arrow in the figure) located at a deviation from the exact Bragg condition ($q_x$) of approximately +1 $\mu m^{-1}$. This type of feature is frequently observed in reciprocal-space maps from defective semiconductor materials and represents a rather large mosaic block whose size starts to approach that of another grain in the crystalline microstructure. Notice that this type of detail could not be discerned from a simple double-axis rocking curve, since extra peaks in such curves are not distinguishable from spurious peaks arising from compositional variations or inadequately filtered $K\beta$ radiation, for example. The value of reciprocal-space mapping is, therefore, its ability to separate out the components contributing to the diffracted intensity, which are unobservable with other diffraction techniques.

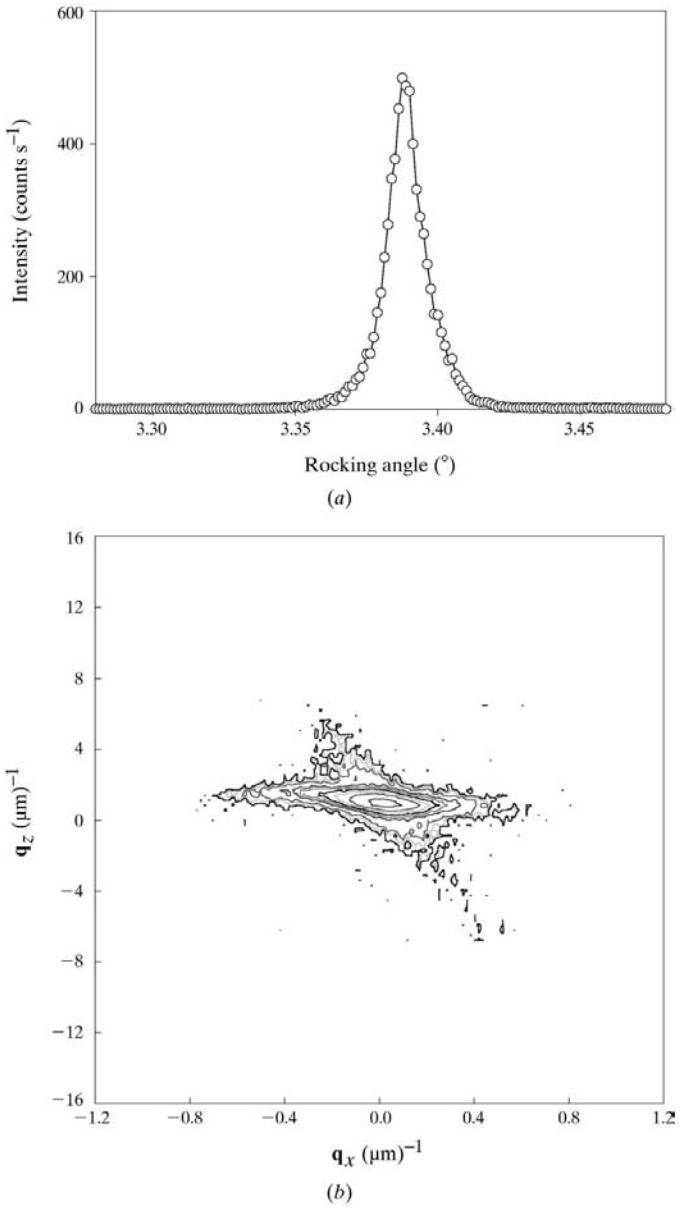


**Figure 6**
X-ray diffraction data from the HEWL (160) reflection. (*a*) Double-axis rocking curve (FWHM = 48 arcsec); (*b*) triple-axis reciprocal-space map.

In addition to the mosaic spread, an intense angled streak of X-ray intensity is also seen. We attribute this feature to the extremely high incident intensity that was generated by the crossed-mirror beam conditioner. An analysis of the X-ray data showed that the reciprocal coordinates of the streak corresponded to the angular position of the sample when it satisfied the Bragg condition, regardless of the angular setting of the analyzer crystal. We believe that the highly intense diffracted beam from the sample propagating towards the analyzer generated parasitic intensity arising from air scatter in our diffractometer system.

As noted in our earlier study (Volz & Matyi, 1999), air scatter from an intense diffracted beam will create parasitic intensity in a reciprocal-space map that is coincident with the analyzer streak that might be expected from a single-reflection analyzer crystal. The off-peak intensity streak remains above background over an angular range that is many times greater than the intrinsic reflecting range of the Ge(004) analyzer crystal used in this work, suggesting that this feature is not a so-called 'analyzer streak' or the convolution of the reflectivity profile of the analyzer crystal with the sample crystal reflection when the latter is oriented on the exact Bragg condition. In future analyses, we plan to flush the beampaths and the sample environment with helium to reduce and hopefully eliminate this parasitic intensity.

Fig. 6 shows the double-axis rocking curve and the triple-axis reciprocal-space map generated by the (160) reflection. A comparison with Fig. 5 indicates that the (160) reciprocal-space map is quite similar to that recorded from the (440) reflection, except that the extra coherently diffracting domain is no longer detectable. Thus, the benefit of obtaining data from multiple reflections before drawing conclusions becomes apparent.

The last reciprocal-space map taken from this sample is shown in Fig. 7, and at first glance is quite different in appearance from those in Figs. 5 and 6. However, this is primarily a consequnce of the trigonometric transformation in (1). The Bragg angles for (440) and (160) are roughly comparable at $\theta_{(440)} = 3.16^\circ$ and $\theta_{(160)} = 3.40^\circ$, compared with $\theta_{(1\bar{2}0)} = 1.25^\circ$.

In Fig. 7, mosaic spread is again evident as a horizontal streak, as is the parasitic scatter streak that is part of the instrument function. However, between these two streaks, another faint streak appears. We suspect that this feature (indicated by an arrow in the figure) represents an inclined surface streak similar to that seen in Fig. 4(*a*). Surface streaks are often seen in high-resolution triple-axis reciprocal-space maps of semiconductor crystals; when a high-quality crystalline lattice is truncated by a flat nearly perfect surface, dynamical diffraction theory predicts the generation of a 'streak' or 'rod' in reciprocal-space of diffracted intensity perpendicular to that surface. If the diffraction planes being studied in the experiment are not perpendicular to the highest quality surface (an asymmetric reflection), the surface streak will appear at an angle in reciprocal space, since this streak will always be perpendicular to the terminating surface. We believe that the {101} facets observed optically on our tetragonal HEWL crystals could be sufficiently perfect to generate surface streaks. Further study is needed to confirm that this is indeed the case.

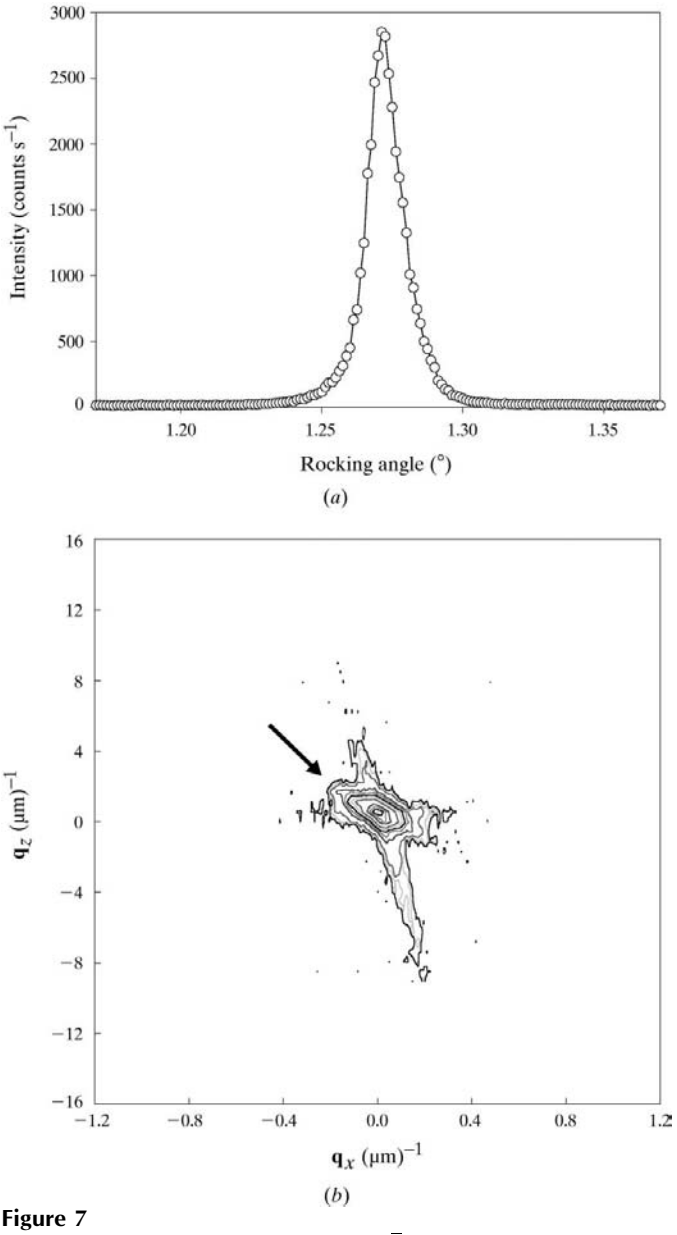


**Figure 7**
X-ray diffraction data from the HEWL ($1\bar{2}0$) reflection. (*a*) Double-axis rocking curve (FWHM = 50 arcsec); (*b*) triple-axis reciprocal-space map map (the arrow indicates the feature discussed in the text).

Also of interest in these three reciprocal-space maps is the absence of features in the longitudinal direction that would indicate strain in the crystals. As shown earlier (Fig. 4*b*), a previously studied HEWL crystal showed a distinctive intensity distribution consistent with a compressive strain in the crystal (Volz & Matyi, 1999). Although that crystal and the one studied in this work were grown in the same laboratory under nominally equivalent conditions, they represent different microdialysis batches. The appearance of reciprocal-space maps from different HEWL crystals with unique strain and mosaic spread signatures is particularly noteworthy because it demonstrates the potential benefit of this high-resolution diffraction technique to the protein crystal growth community in terms of characterizing the defects in protein crystals.

## 5. Discussion

One result of the present investigation is that it demonstrates that X-ray diffraction methods with high angular resolution (specifically, high-resolution triple-axis reciprocal-space mapping) can be successfully applied to protein crystals in a laboratory environment. While the availability of (for instance) a synchrotron source would be likely to reduce the time required to record a reciprocal-space map, our study suggests that any well equipped protein crystallography laboratory should be able to perform studies of the relation between crystal-growth protocols and the subsequent structural perfection of macromolecular crystals. It is precisely this type of close feedback between the crystal-growth and characterization activities in the semiconductor industry that has enabled rapid progress in that community. We believe that the ability to perform defect analyses in a laboratory environment, closely coupled to the crystal-growth process, can lead to an improvement in protein crystal quality and ultimately in protein structure determinations as well.

As discussed previously, two of the five reciprocal-space maps have features that would be consistent with the presence of a dynamical surface streak from an asymmetric reflection; however, this condition presupposes that the crystal will diffract according to the dynamical theory of diffraction. This will only be the case if the crystal is both (i) relatively structurally perfect and (ii) large in extent when compared with the extinction distance $\xi$ defined (Bowen & Tanner, 1998) as

$$\xi = V_C/(r_o C|F_h|\lambda), \qquad (2)$$

where $C$ is the polarization factor, $V_C$ is the volume of the unit cell (239.7 nm$^3$ for tetragonal HEWL; Volz & Matyi, 1999), $r_o$ is the classical electron radius, $|F_h|$ is the amplitude of the structure factor and $\lambda$ is the X-ray wavelength. The magnitude of the extinction distance provides a measure of the crystal

size that is required to establish a dynamic coupling between the incident and diffracted wavefields inside a crystal. A crystal that is large in comparison with $\xi$ and relatively defect-free will permit the two wavefields to couple and allows the diffraction process to proceed according to the dynamic theory. In contrast, a crystal that is small with respect to the extinction distance will not allow the incident and diffracted wavefields to couple sufficiently for dynamic effects to occur. The result is that a crystal that is small in comparison to $\xi$ will be expected to diffract kinematically. Similarly, kinematic diffraction also dominates in a structurally defective crystal, where defects disrupt the wavefields traveling through the crystal and prevent their coupling.

Owing to the large unit cell and relatively small magnitude of the structure factor in protein crystals, the value of $\xi$ in crystals such as HEWL is rather large. Otalora *et al.* (1999) have estimated an average value for the structure factor of approximately 596 electrons. Using this value with a polarization factor $C = 1$ and 1.54 Å Cu $K\alpha$ radiation, we calculate an extinction distance of 0.9 mm. This value is in good agreement with estimates of the extinction distance reported by Fourme *et al.* (1995) and Helliwell (1988). Thus, a typical HEWL crystal (sub-millimeter in size) would be expected to exhibit both dynamical and kinematical diffraction characteristics.

In order to interpret high-resolution diffraction data it would be useful to predict the diffraction characteristics of HEWL crystals. If the crystal is diffracting dynamically, then the rocking-curve width in the symmetric Laue (transmission) geometry is given (Bowen & Tanner, 1998) by

$$\Delta\theta = \frac{2|C||\chi_h|}{\sin 2\theta} = \frac{2\lambda}{\pi\xi \sin 2\theta}, \tag{3}$$

where $\chi_h$ ($= -F_h r_o \lambda^2/\pi V_C$) is the $h$ component of the Fourier expansion of the electric susceptibility. Using this expression for the HEWL (440) reflection, we calculate an extremely narrow rocking-curve FWHM of about 0.2 arcsec. Again, this is in agreement with similar calculations by Fourme *et al.* (1995) and Helliwell (1988).

Now we examine the expected rocking-curve width in the kinematic limit. If the crystal were infinite in extent, of course, the kinematic theory predicts that the Bragg reflection should be a delta function. For a non-infinite crystal, the expected rocking-curve width can be determined from the well known interference function

$$\begin{aligned} J &= \sum_0^{N_1-1} \exp(2\pi i N_1 q_1) \sum_0^{N_2-1} \exp(2\pi i N_2 q_2) \sum_0^{N_3-1} \exp(2\pi i N_3 q_3) \\ &= \frac{\sin^2(\pi N_1 q_1)}{\sin^2(\pi q_1)} \frac{\sin^2(\pi N_2 q_2)}{\sin^2(\pi q_2)} \frac{\sin^2(\pi N_3 q_3)}{\sin^2(\pi q_3)}, \end{aligned} \tag{4}$$

where $q$ is the deviation from the Bragg condition (in radians) in a crystal containing $N = N_1 N_2 N_3$ unit cells. For a 0.5 mm crystal with a unit-cell size of 50 Å, (4) predicts a kinematic FWHM of 1.8 arcsec. The similarity between the dynamic and kinematic rocking-curve widths for protein crystals is very different from the situation with inorganic materials, where the combination of a relatively small unit cell (<10 Å), a small extinction distance (of the order of several micrometers) and a large bulk crystal size makes the kinematic rocking-curve width much smaller than the dynamic FWHM calculated from (3). Thus, we are led to the conclusion that protein crystals lie at the convergence of the kinematic (ideally imperfect) and dynamic (ideally perfect) treatments of diffraction. From a physical point of view, it would be difficult to establish a dynamic coupling between the incident and diffracted wavefields in a high-quality (ideally defect-free) protein crystal, owing to the low amplitude of the scattered X-rays and the combination of a large unit cell and a small macroscopic crystal size.

The effects of the apparent confluence of dynamic and kinematic behavior can be found in the properties of surface streaks generated by protein crystals. As mentioned earlier, in dynamically diffracting materials the surface streak represents the intrinsic reflectivity profile of the crystal and is thus commonly seen in high-resolution reciprocal-space maps from high-quality structures. However, the truncation of an otherwise infinite lattice is also expected to generate a surface streak within the framework of the kinematic theory. For instance, Robinson (1986) has shown that for a crystal that is infinite in two directions (say, $q_1$ and $q_2$) and finite in the third $q_3$ direction, the interference function in (4) can be written as

$$J' = N_1^2 N_2^2 \frac{\sin^2(\pi N_3 q_3)}{\sin^2(\pi q_3)}, \tag{5}$$

which will result in a $1/(\Delta q)^2$ dependence of the intensity of the Bragg peak in the $q_3$ direction. Therefore, even in the kinematic limit, a 'surface streak' of intensity would be anticipated from a spatially truncated crystal. At this point, it is not clear whether the extra features seen in Figs. 5(*b*) and 8 arise from dynamic or kinematic diffraction; further work is needed to fully understand these characteristics.

We are thus led to the conclusion that protein X-ray crystallography represents an interesting intellectual puzzle, since the behavior of these crystals appears to lie at the convergence of the kinematic and dynamic theories. While it is clear that this apparent duality has an impact on the 'appearance' of protein crystals in high-resolution defect analyses, we also speculate that it may influence structural crystallography as well. Similar observations have been made by others (Helliwell, 1988; Fourme *et al.*, 1995; Otalora *et al.*, 1999) and it appears that further analysis of the questions regarding kinematic *versus* dynamic diffraction are needed.

## 6. Conclusions

This work has demonstrated that high-resolution X-ray reciprocal-space mapping, a widely used technique for the characterization of semiconductor crystals, can be successfully applied to more structurally imperfect protein crystals. Furthermore, this work can be performed in a conventional laboratory environment; the use of a synchrotron source is not

required. Future work will concentrate on a better understanding of the intensity distribution seen in the transmission geometry from protein crystals with varying degrees of structural perfection as well as understanding their diffraction characteristics as the two limiting theories of X-ray diffraction converge. It is anticipated that qualitative and semi-quantitative knowledge of the strain and mosaicity introduced in HEWL crystals can lead to a better understanding of the defect structure in protein crystals, which is a necessary first step towards defect elimination.

Support for this work came from the University of Wisconsin Graduate School and from NASA (Microgravity Sciences Division) *via* grant NCC8-53 and the National Science Foundation *via* grant DMR-9319421. HMV acknowledges support from an NSF Graduate Research Fellowship and an International Centre for Diffraction Data Scholarship.

## References

Bowen, D. K. & Tanner, B. K. (1998). *High Resolution X-ray Diffractometry and Topography*. Bristol, PA: Taylor & Francis.
Branden, C. & Tooze, J. (1999). *Introduction to Protein Structure*, 2nd ed. New York: Garland.
Colapietro, M., Cappuccio, G., Marciante, C., Pifferi, A., Spagna, R. & Helliwell, J. R. (1992). *J. Appl. Cryst.* **25**, 192–194.
Dobrianov, I., Caylor, C., Lemay, S. G., Finkelstein, K. D. & Thorne, R. E. (1999). *J. Cryst. Growth*, **196**, 511–523.
Drenth, J. (1999). *Principles of Protein X-ray Crystallography*, 2nd ed. New York: Springer–Verlag.
Fourme, R., Ducruix, A., Ries-Kautt, M. & Capelle, R. (1995). *J. Synchrotron Rad.* **2**, 136–142.
Helliwell, J. R. (1988). *J. Cryst. Growth*, **90**, 259–272.
Izumi, K., Sawamura, S. & Ataka, M. (1996). *J. Cryst. Growth*, **168**, 106–110.
Loxley, N. (1994). *III–Vs Rev.* **7**, 59–63.
Loxley, N., Tanner, B. K. & Bowen, D. K. (1995). *Adv. X-ray Anal.* **38**, 361–365.
McPherson, A. (1999). *Crystallization of Biological Macromolecules.* New York: Cold Spring Harbor Laboratory Press.
Matyi, R. J., Moran, P. D., Hagquist, W. W. D. & Volz, H. M. (2000). In the press.
Otalora, F., Garcia-Ruiz, J. M., Gavira, J. A. & Capelle, B. (1999). *J. Cryst. Growth*, **196**, 546–558.
Robinson, I. K. (1986). *Phys. Rev. B*, **33**, 3830–3836.
Shaikevitch, A. & Kam, Z. (1981). *Acta Cryst.* A**37**, 871–875.
Snell, E. H., Weisgerber, S., Helliwell, J. R., Weckert, E., Hölzer, K. & Schroer, K. (1995). *Acta Cryst.* D**51**, 1099–1102.
Stojanoff, V. & Siddons, D. P. (1996). *Acta Cryst.* A**52**, 498–499.
Stojanoff, V., Siddons, D. P., Monaco, L. A., Vekilov, P. & Rosenberger, F. (1997). *Acta Cryst.* D**53**, 588–595.
Volz, H. M. & Matyi, R. J. (1999). *Philos. Trans. R. Soc. London Ser. A*, **357**, 2789–2799.